

LENGTH PRESERVING NUMERICAL SCHEMES FOR THE NEMATIC LIQUID CRYSTAL FLOWS

RUONAN CAO^{1,*}  AND NIANYU YI^{1,2} 

Abstract. In this paper, we introduce two novel classes of length preserving schemes for the Ericksen–Leslie model based on two distinct Lagrange multiplier approaches. In the first approach, the Lagrange multiplier $q(\mathbf{x}, t)$ is defined as $|\nabla \mathbf{d}|^2$ at the continuous level. In the second approach, $q(\mathbf{x}, t)$ is introduced at the discrete level to enforce the length constraint, while it remains identically zero at the continuous level. Within a predictor-corrector framework, we develop efficient and robust second-order length preserving schemes for the Ericksen–Leslie model. A series of numerical experiments are presented to verify the accuracy, stability, and energy dissipation properties of the proposed schemes. In addition, numerical comparisons show that our schemes achieve significantly improved computational efficiency compared to the existing method.

Mathematics Subject Classification. 65M22, 65M60, 65Z05, 76A15.

Received April 8, 2025. Accepted September 25, 2025.

1. INTRODUCTION

We consider the simplified Ericksen–Leslie model in the following form, as described in [15],

$$\begin{cases} \frac{\partial \mathbf{d}}{\partial t} + \mathbf{u} \cdot \nabla \mathbf{d} - \gamma \Delta \mathbf{d} - \gamma |\nabla \mathbf{d}|^2 \mathbf{d} = 0, & (1.1) \\ \frac{\partial \mathbf{u}}{\partial t} + \mathbf{u} \cdot \nabla \mathbf{u} - \nu \Delta \mathbf{u} + \nabla p + \lambda \nabla \cdot \left((\nabla \mathbf{d})^t \nabla \mathbf{d} \right) = 0, & (1.2) \\ \nabla \cdot \mathbf{u} = 0, & (1.3) \\ |\mathbf{d}| = 1, & (1.4) \end{cases}$$

in $\Omega_T = \Omega \times (0, T]$, where $\Omega \subset \mathbb{R}^d$ ($d = 2, 3$) is a bounded domain with a Lipschitz continuous boundary $\partial\Omega$. Boundary conditions are prescribed as

$$\mathbf{u}|_{\partial\Omega} = 0, \quad \partial_{\mathbf{n}} \mathbf{d}|_{\partial\Omega} = 0.$$

The unknowns are the velocity field \mathbf{u} , pressure p , and director field \mathbf{d} , which characterizes the orientation of liquid crystal molecules. The physical parameters include fluid viscosity ν , elasticity constant λ , and relaxation

Keywords and phrases. Nematic liquid crystal flows, Ericksen–Leslie model, Lagrange multiplier, length preserving, predictor-corrector, pressure-correction.

¹ School of Mathematics and Computational Science, Xiangtan University, Xiangtan 411105, P.R. China.

² Hunan Key Laboratory for Computation and Simulation in Science and Engineering, Xiangtan University, Xiangtan 411105, P.R. China.

*Corresponding author: ruonan9cao@163.com

time γ . An important property of system (1.1)–(1.4) is that the director field \mathbf{d} satisfies the length preserving condition

$$|\mathbf{d}(\mathbf{x}, t)| = 1, \quad \forall \mathbf{x} \in \Omega.$$

The system (1.1)–(1.4) inherently satisfies an energy dissipation law. Let $\|\cdot\|$ denote the L^2 norm of scalars, vectors or tensors, and (\cdot, \cdot) means the L^2 inner product. By taking the inner product of (1.1) with $\lambda(-\Delta \mathbf{d} - |\nabla \mathbf{d}|^2 \mathbf{d})$ and (1.2) with \mathbf{u} , and summing the results with some algebraic manipulation, we find that the above system (1.1)–(1.4) satisfies the following energy dissipation law:

$$\frac{d}{dt} E(\mathbf{u}, \mathbf{d}) = -\nu \|\nabla \mathbf{u}\|^2 - \lambda \gamma \|\Delta \mathbf{d} + |\nabla \mathbf{d}|^2 \mathbf{d}\|^2,$$

where

$$E(\mathbf{u}, \mathbf{d}) = \frac{1}{2} \|\mathbf{u}\|^2 + \frac{\lambda}{2} \|\nabla \mathbf{d}\|^2.$$

The Ericksen–Leslie model, developed by Ericksen [5, 6] and Leslie [12, 13], provides a hydrodynamic framework for modeling nematic liquid crystals. It consists of coupled macroscopic equations incorporating the Oseen–Frank elastic theory, which governs steady-state and equilibrium solutions [11, 13, 19]. The Ericksen–Leslie model plays a fundamental role in understanding the hydrodynamics of nematic liquid crystals, which have practical applications in various technologies such as liquid crystal displays (LCDs), optical devices, and biosensors. Accurate and stable numerical schemes are essential for reliably simulating and optimizing liquid crystal systems, especially when defect dynamics and constraint enforcement are critical. Due to the complexity of the original model, which involves various reaction-coupling terms, Lin [15] proposed the simplified version (1.1)–(1.4). Numerous theoretical analyses and numerical simulation have been conducted on the simplified Ericksen–Leslie model (1.1)–(1.4). Notably, Lin and Liu [16] derived several energy laws and established the global existence theorem of weak solutions. Du *et al.* [4] investigated a Fourier-spectral method, establishing its convergence and deriving an error estimate that confirms its spectral accuracy. Additionally, Lin and Liu [17] presented a C^0 finite element method for the 2D hydrodynamic liquid crystal model.

The desire to design a numerical method that can preserve the intrinsic properties of the Ericksen–Leslie model stems not only from the need to render numerical approximations physically meaningful, but also from the goal of enhancing the robustness and accuracy of the numerical scheme. Usually it is difficult to obtain linear and decoupled numerical schemes for the Ericksen–Leslie model which preserve the length constraint $|\mathbf{d}| = 1$. Existing numerical approaches for handling the length constraint can be broadly classified into three categories: (i) penalty method [16], this approach employs the Ginzburg–Landau penalty function to relax the constraint $|\mathbf{d}| = 1$. Liu and Walkington [18] analyzed the finite element approximation of liquid crystal flows using the Ginzburg–Landau penalty function, deriving convergence results and ε -dependent error estimates for the penalized system. Other works such as [2, 7] also adopt this framework, but the constraint is only approximately satisfied. (ii) operator-splitting method, in this approach, an approximate solution is first computed without enforcing the constraint. A simple projection is then applied to enforce $|\mathbf{d}| = 1$. Glowinski *et al.* [8] proposed a time-splitting scheme based on the projection method for the director vector only problem (*i.e.*, problem (1.1) and (1.4) with $\mathbf{u} = 0$). (iii) Lagrange multiplier method, a Lagrange multiplier q is introduced to enforce the length constraint. For example, Badia *et al.* [1] developed a finite element method based on a saddle-point formulation, introducing a Lagrange multiplier to enforce the length constraint $|\mathbf{d}| = 1$.

Although the above penalty method yields reasonable numerical results, it only approximates the constraint and is sensitive to the penalty parameter. The simple projection of the operator-splitting method is easy to implement but may cause discontinuities and affect energy stability, especially near singularities. The Lagrange multiplier method offers a more rigorous variational framework that better preserves the constraint and enhances stability. However, developing efficient and fully decoupled schemes based on this method, especially with second-order accuracy in time, remains a challenge.

Recently, Cheng and Shen [3] proposed a novel Lagrange multiplier method based on the predictor-corrector framework to design efficient, robust, and length preserving higher-order algorithms for the Landau–Lifshitz

equation. Motivated by this work, we aim to develop fully decoupled and length preserving schemes for the Ericksen–Leslie model (1.1)–(1.4). In summary, we first introduce two types of Lagrange multipliers within the predictor-corrector framework to solve (1.1) and (1.4). Next, the pressure-correction (PC) approach [9] is employed to decouple the system (1.2) and (1.3). Finally, we propose two fully decoupled, length preserving schemes for the Ericksen–Leslie model. To the best of our knowledge, these are the first fully decoupled and length preserving second-order schemes for the Ericksen–Leslie model (1.1)–(1.4). Each scheme employs an additional space-independent Lagrange multiplier to strictly enforce the length constraint.

This paper is organized as follows. In Section 2, we present two formulations of the Ericksen–Leslie model (1.1)–(1.4) by introducing Lagrange multipliers to enforce the length constraint. In Section 3, we construct two classes of robust and accurate length preserving time discretization schemes based on predictor-corrector and pressure-correction approach. In Section 4, we present some numerical experiments to validate the stability and accuracy for the proposed schemes and compare their performance with that of the scheme in [1].

2. FORMULATIONS OF ERICKSEN–LESLIE MODEL WITH LAGRANGE MULTIPLIERS

We begin by noting that the elastic stress tensor can be reformulated as follows [16]:

$$\lambda \nabla \cdot \left((\nabla \mathbf{d})^t \nabla \mathbf{d} \right) = \frac{\lambda}{2} \nabla (|\nabla \mathbf{d}|^2) + \lambda (\nabla \mathbf{d})^t \Delta \mathbf{d},$$

where $\frac{\lambda}{2} |\nabla \mathbf{d}|^2$ can be incorporated as part of the pressure. Using this reformulation, the simplified Ericksen–Leslie model (1.1)–(1.4) can be rewritten in the following form:

$$\begin{cases} \frac{\partial \mathbf{d}}{\partial t} + \mathbf{u} \cdot \nabla \mathbf{d} - \gamma \Delta \mathbf{d} - \gamma |\nabla \mathbf{d}|^2 \mathbf{d} = 0, & (2.1) \\ \frac{\partial \mathbf{u}}{\partial t} + \mathbf{u} \cdot \nabla \mathbf{u} - \nu \Delta \mathbf{u} + \nabla p + \lambda (\nabla \mathbf{d})^t \Delta \mathbf{d} = 0, & (2.2) \\ \nabla \cdot \mathbf{u} = 0, & (2.3) \\ |\mathbf{d}| = 1. & (2.4) \end{cases}$$

Then we introduce two types of Lagrange multipliers to enforce the length constraint, leading to two equivalent formulations of the Ericksen–Leslie model.

2.1. Lagrange multiplier I

We consider a Lagrange multiplier $q(\mathbf{x}, t)$ as in [1] to enforce the length constraint. Using the identity

$$\frac{1}{2} \Delta |\mathbf{d}|^2 = \mathbf{d} \cdot \Delta \mathbf{d} + |\nabla \mathbf{d}|^2,$$

we find that

$$-\mathbf{d} \cdot \Delta \mathbf{d} = |\nabla \mathbf{d}|^2, \quad \text{if } |\mathbf{d}| = 1. \tag{2.5}$$

Hence, we can rewrite (2.1)–(2.4) with $|\mathbf{d}| = 1$ in the following equivalent form:

$$\begin{cases} \frac{\partial \mathbf{d}}{\partial t} = -\mathbf{u} \cdot \nabla \mathbf{d} + \gamma (\Delta \mathbf{d} + q(\mathbf{x}, t) \mathbf{d}), & (2.6) \\ \frac{\partial \mathbf{u}}{\partial t} + (\mathbf{u} \cdot \nabla) \mathbf{u} - \nu \Delta \mathbf{u} + \nabla p + \lambda (\nabla \mathbf{d})^t \Delta \mathbf{d} = 0, & (2.7) \\ \nabla \cdot \mathbf{u} = 0, & (2.8) \\ |\mathbf{d}| = 1. & (2.9) \end{cases}$$

Indeed, multiplying (2.6) by \mathbf{d} and utilizing (2.5) along with the condition $|\mathbf{d}| = 1$, it follows that $q = |\nabla \mathbf{d}|^2$. Hence q can also be viewed as the Lagrange multiplier for the constraint $|\mathbf{d}| = 1$.

By taking the inner product of (2.6) with $\lambda(-\Delta \mathbf{d} - q\mathbf{d})$ and (2.7) with \mathbf{u} , and summing the results with some algebraic manipulation, we obtain the following energy dissipation law for the system (2.6)–(2.9):

$$\frac{d}{dt}E(\mathbf{u}, \mathbf{d}) = -\nu\|\nabla\mathbf{u}\|^2 - \lambda\gamma\|\Delta\mathbf{d} + q\mathbf{d}\|^2,$$

where

$$E(\mathbf{u}, \mathbf{d}) = \frac{1}{2}\|\mathbf{u}\|^2 + \frac{\lambda}{2}\|\nabla\mathbf{d}\|^2.$$

Note that the coupling term involving the Lagrange multiplier vanishes under the length constraint

$$(\mathbf{u} \cdot \nabla \mathbf{d}, q\mathbf{d}) = ((\nabla \mathbf{d})^t q\mathbf{d}, \mathbf{u}) = \left(\frac{1}{2}q\nabla|\mathbf{d}|^2, \mathbf{u} \right) = 0, \quad \text{if } |\mathbf{d}| = 1.$$

2.2. Lagrange multiplier II

Following the approach in [3], we reformulate the Ericksen–Leslie model by introducing a Lagrange multiplier $q(\mathbf{x}, t)$ to enforce the length constraint.

$$\begin{cases} \frac{\partial \mathbf{d}}{\partial t} = -\mathbf{u} \cdot \nabla \mathbf{d} + \gamma(\Delta \mathbf{d} + |\nabla \mathbf{d}|^2 \mathbf{d}) + q(\mathbf{x}, t)\mathbf{d}, & (2.10) \\ \frac{\partial \mathbf{u}}{\partial t} + (\mathbf{u} \cdot \nabla)\mathbf{u} - \nu\Delta \mathbf{u} + \nabla p + \lambda(\nabla \mathbf{d})^t \Delta \mathbf{d} = 0, & (2.11) \\ \nabla \cdot \mathbf{u} = 0, & (2.12) \\ |\mathbf{d}| = 1. & (2.13) \end{cases}$$

Obviously the above system is equivalent to (2.1)–(2.4) in the case $q(\mathbf{x}, t) = 0$. However, we can directly discretize (2.10) and (2.13) by explicitly performing $|\mathbf{d}| = 1$. The initial conditions are prescribed as follows:

$$\mathbf{u}(\mathbf{x}, 0) = \mathbf{u}_0(\mathbf{x}), \quad \mathbf{d}(\mathbf{x}, 0) = \mathbf{d}_0(\mathbf{x}), \quad \text{for } \mathbf{x} \in \Omega,$$

where $\mathbf{u}_0 : \Omega_T \rightarrow \mathbb{R}^d$ and $\mathbf{d}_0 : \Omega_T \rightarrow \mathbb{R}^d$ are given functions.

3. LENGTH PRESERVING TIME DISCRETIZATION SCHEMES FOR THE ERICKSEN–LESLIE MODEL

In this section, we develop semi-discrete schemes for the reformulated Ericksen–Leslie models (2.6)–(2.9) and (2.10)–(2.13), respectively. For clarity, the scheme derived from (2.6) to (2.9) is denoted by LM-I, and those based on (2.10)–(2.13) is denoted by LM-II. Let $\{t^n | t^n = n\delta t, n = 0, 1, \dots, N\}$ represent a uniform partition of the interval $[0, T]$, where $\delta t = T/N$ is the time step and N is a positive integer.

3.1. Length preserving schemes *via* Lagrange multiplier I

We propose a class of efficient, fully decoupled, and length preserving numerical semi-discrete schemes for the system (2.6)–(2.9). These schemes are constructed based on a predictor-corrector (PC) strategy. The key idea is inspired by the analogy between the Lagrange multiplier $q(\mathbf{x}, t)$, which enforces the length constraint, and the pressure term (resp. incompressibility constrain) in the Navier–Stokes equations. Hence we can adopt the operator splitting and pressure-correction approaches for solving (2.6) and (2.9). The same PC strategy is also employed to decouple the velocity and pressure in (2.7) and (2.8). As a result, we obtain a class of fully decoupled and length preserving schemes that are both efficient and easy to implement.

3.1.1. LM-I first-order scheme (LM-I-1st)

We first introduce a first-order, fully decoupled semi-discrete scheme based on the predictor-corrector framework. Given $\mathbf{u}^n, \mathbf{d}^n$ and p^n , the solution at t^{n+1} is computed through the following steps:

– Step 1 (Predictor): Find \mathbf{d}_*^{n+1} satisfying

$$\frac{\mathbf{d}_*^{n+1} - \mathbf{d}^n}{\delta t} = -(\mathbf{u}^n \cdot \nabla)\mathbf{d}^n + \gamma\Delta\mathbf{d}_*^{n+1}. \tag{3.1}$$

– Step 2 (Corrector): Find $(\mathbf{d}^{n+1}, q^{n+1})$

$$\frac{\mathbf{d}^{n+1} - \mathbf{d}_*^{n+1}}{\delta t} = \gamma q^{n+1} \mathbf{d}^{n+1}, \tag{3.2}$$

$$|\mathbf{d}^{n+1}| = 1. \tag{3.3}$$

– Step 3: Find \mathbf{u}_*^{n+1} satisfying

$$\frac{\mathbf{u}_*^{n+1} - \mathbf{u}^n}{\delta t} + (\mathbf{u}^n \cdot \nabla)\mathbf{u}_*^{n+1} - \nu\Delta\mathbf{u}_*^{n+1} + \nabla p^n + \lambda(\nabla\mathbf{d}^{n+1})^t\Delta\mathbf{d}^{n+1} = 0, \quad \mathbf{u}_*^{n+1}|_{\partial\Omega} = 0. \tag{3.4}$$

– Step 4: Find $(\mathbf{u}^{n+1}, p^{n+1})$ satisfying

$$\frac{\mathbf{u}^{n+1} - \mathbf{u}_*^{n+1}}{\delta t} + \nabla(p^{n+1} - p^n) = 0, \tag{3.5}$$

$$\nabla \cdot \mathbf{u}^{n+1} = 0, \quad \mathbf{u}^{n+1} \cdot \mathbf{n}|_{\partial\Omega} = 0. \tag{3.6}$$

Theorem 3.1. *Assuming $\|\Delta^2 \mathbf{d}^n\|_{L^2} \leq C_1$, $\|\Delta^2(\mathbf{u}^n \cdot \nabla \mathbf{d}^n)\|_{L^2} \leq C_1$ and δt is sufficiently small, the scheme (3.2) and (3.3) admits two distinct sets of solutions due to the coupling between \mathbf{d}^{n+1} and q^{n+1} . The solution set consistent with (2.6) and (2.9) is given by*

$$q^{n+1} = \frac{1 - |\mathbf{d}_*^{n+1}|}{\gamma\delta t}, \tag{3.7}$$

and

$$\mathbf{d}^{n+1} = \frac{\mathbf{d}_*^{n+1}}{|\mathbf{d}_*^{n+1}|}, \tag{3.8}$$

where C_1 is a positive constant.

Proof. Rewriting (3.2), we obtain

$$(1 - \delta t\gamma q^{n+1})\mathbf{d}^{n+1} = \mathbf{d}_*^{n+1}. \tag{3.9}$$

Squaring both sides in (3.9) and using the constraint $|\mathbf{d}^{n+1}| = 1$, we obtain

$$(1 - \delta t\gamma q^{n+1})^2 = |\mathbf{d}_*^{n+1}|^2.$$

This equation admits two possible solutions

$$q^{n+1} = \frac{1 - |\mathbf{d}_*^{n+1}|}{\delta t\gamma} \quad \text{or} \quad q^{n+1} = \frac{1 + |\mathbf{d}_*^{n+1}|}{\delta t\gamma}.$$

We now show that only $q^{n+1} = \frac{1 - |\mathbf{d}_*^{n+1}|}{\delta t\gamma}$ satisfies the required constraints.

From (3.1), it follows that

$$\mathbf{d}_*^{n+1} = (I - \delta t \gamma \Delta)^{-1}(\mathbf{d}^n - \delta t(\mathbf{u}^n \cdot \nabla)\mathbf{d}^n).$$

By formally expanding the inverse operator, we obtain

$$(I - \delta t \gamma \Delta)^{-1} = I + \delta t \gamma \Delta + \delta t^2 \gamma^2 \Delta^2 + \dots,$$

which yields the expression

$$\mathbf{d}_*^{n+1} = (I + \delta t \gamma \Delta)(\mathbf{d}^n - \delta t(\mathbf{u}^n \cdot \nabla)\mathbf{d}^n) + \mathcal{R},$$

where the remainder term \mathcal{R} is given by

$$\mathcal{R} = [(\delta t \gamma \Delta)^2 + (\delta t \gamma \Delta)^3 + \dots](\mathbf{d}^n - \delta t(\mathbf{u}^n \cdot \nabla)\mathbf{d}^n).$$

This implies that

$$\|\mathcal{R}\|_{L^2} \leq C \delta t^2,$$

for some constant C depending on γ and C_1 .

Consequently, we have

$$\begin{aligned} |\mathbf{d}_*^{n+1}|^2 &= |(I + \delta t \gamma \Delta)(\mathbf{d}^n - \delta t(\mathbf{u}^n \cdot \nabla)\mathbf{d}^n)|^2 + \mathcal{O}(\delta t^2) \\ &= |\mathbf{d}^n - \delta t(\mathbf{u}^n \cdot \nabla)\mathbf{d}^n|^2 + \delta t^2 \gamma^2 |\Delta(\mathbf{d}^n - \delta t(\mathbf{u}^n \cdot \nabla)\mathbf{d}^n)|^2 \\ &\quad + 2\delta t \gamma (\mathbf{d}^n - \delta t(\mathbf{u}^n \cdot \nabla)\mathbf{d}^n) \cdot \Delta(\mathbf{d}^n - \delta t(\mathbf{u}^n \cdot \nabla)\mathbf{d}^n) + \mathcal{O}(\delta t^2). \end{aligned} \tag{3.10}$$

Next, we estimate each term on the right-hand side of (3.10) individually. Using identity (2.5) and the fact that

$$\mathbf{u} \cdot \nabla \mathbf{d} \cdot \mathbf{d} = \frac{1}{2} \mathbf{u} \cdot \nabla |\mathbf{d}|^2 = 0,$$

we deduce that

$$\begin{aligned} |\mathbf{d}^n - \delta t(\mathbf{u}^n \cdot \nabla)\mathbf{d}^n|^2 &= 1 - 2\delta t \mathbf{u}^n \cdot \nabla \mathbf{d}^n \cdot \mathbf{d}^n + \delta t^2 |(\mathbf{u}^n \cdot \nabla \mathbf{d}^n)|^2 \\ &= 1 + \mathcal{O}(\delta t^2), \end{aligned} \tag{3.11}$$

$$\begin{aligned} 2\delta t \gamma (\mathbf{d}^n - \delta t(\mathbf{u}^n \cdot \nabla)\mathbf{d}^n) \cdot \Delta(\mathbf{d}^n - \delta t(\mathbf{u}^n \cdot \nabla)\mathbf{d}^n) &= 2\delta t \gamma (\mathbf{d}^n - \mathcal{O}(\delta t)) \cdot \Delta(\mathbf{d}^n - \mathcal{O}(\delta t)) \\ &= 2\delta t \gamma \mathbf{d}^n \cdot \Delta \mathbf{d}^n + \mathcal{O}(\delta t^2) \\ &= -2\delta t \gamma |\nabla \mathbf{d}^n|^2 + \mathcal{O}(\delta t^2). \end{aligned} \tag{3.12}$$

For the second term on the right-hand side of (3.10), we consider a projection decomposition. Given a unit vector $\mathbf{d}^n \in \mathbb{R}^d$ such that $|\mathbf{d}^n| = 1$, any vector $\mathbf{v} \in \mathbb{R}^d$ can be uniquely decomposed into a tangential and a normal component with respect to \mathbf{d}^n as follows:

$$\mathbf{v} = (\mathbf{v} \cdot \mathbf{d}^n)\mathbf{d}^n + (\mathbf{v} - (\mathbf{v} \cdot \mathbf{d}^n)\mathbf{d}^n).$$

Taking the norm on both sides and noting that $|\mathbf{d}^n| = 1$, we obtain

$$|\mathbf{v}|^2 = (\mathbf{v} \cdot \mathbf{d}^n)^2 + |\mathbf{v} - (\mathbf{v} \cdot \mathbf{d}^n)\mathbf{d}^n|^2.$$

Letting $\mathbf{v} = \Delta \mathbf{d}^n$, and using identity (2.5), we deduce that

$$|\Delta \mathbf{d}^n|^2 = (\Delta \mathbf{d}^n \cdot \mathbf{d}^n)^2 + |\Delta \mathbf{d}^n - (\Delta \mathbf{d}^n \cdot \mathbf{d}^n)\mathbf{d}^n|^2 = |\nabla \mathbf{d}|^4 + |\Delta \mathbf{d}^n - (\Delta \mathbf{d}^n \cdot \mathbf{d}^n)\mathbf{d}^n|^2.$$

Hence, the second term on the right-hand side of (3.10) satisfies

$$\delta t^2 \gamma^2 |\Delta(\mathbf{d}^n - \delta t(\mathbf{u}^n \cdot \nabla)\mathbf{d}^n)|^2 = \delta t^2 \gamma^2 |\Delta \mathbf{d}^n|^2 + \mathcal{O}(\delta t^2) = \delta t^2 \gamma^2 |\nabla \mathbf{d}^n|^4 + \mathcal{O}(\delta t^2). \quad (3.13)$$

Applying equations (3.11)–(3.13), the expression (3.10) can be simplified as

$$|\mathbf{d}_*^{n+1}|^2 \approx 1 - 2\delta t \gamma |\nabla \mathbf{d}^n|^2 + \delta t^2 \gamma^2 |\nabla \mathbf{d}^n|^4 = (1 - \delta t |\nabla \mathbf{d}^n|^2)^2.$$

Consequently, the Lagrange multiplier q^{n+1} defined by

$$q^{n+1} = \frac{1 - |\mathbf{d}_*^{n+1}|}{\delta t},$$

can be approximated as

$$q^{n+1} \approx \frac{1 - (1 - \delta t \gamma |\nabla \mathbf{d}^n|^2)}{\delta t \gamma} = |\nabla \mathbf{d}^n|^2,$$

which is consistent with the continuous level identity

$$q(\mathbf{x}, t) = -\Delta \mathbf{d} \cdot \mathbf{d} = |\nabla \mathbf{d}|^2,$$

under the constraint $|\mathbf{d}| = 1$.

Substituting $q^{n+1} = \frac{1 - |\mathbf{d}_*^{n+1}|}{\gamma \delta t}$ into (3.2), we obtain $\mathbf{d}^{n+1} = \frac{\mathbf{d}_*^{n+1}}{|\mathbf{d}_*^{n+1}|}$. □

Remark 3.1. In *Step 4*, we decouple \mathbf{u}^{n+1} and p^{n+1} by considering (3.5) and (3.6) through the following steps: Taking divergence on both sides of the equation (3.5), we obtain

$$\Delta(p^{n+1} - p^n) = \frac{1}{\delta t} \nabla \cdot \mathbf{u}_*^{n+1}. \quad (3.14)$$

Finally, \mathbf{u}^{n+1} is updated by

$$\mathbf{u}^{n+1} = \mathbf{u}_*^{n+1} - \delta t \nabla(p^{n+1} - p^n). \quad (3.15)$$

3.1.2. LM-I second-order backward difference formula scheme (LM-I-BDF2)

We present a second-order predictor-corrector (PC) scheme for solving the system (2.6)–(2.9). Extending the LM-I-1st scheme, this scheme employs a predictor-corrector strategy to achieve second-order accuracy while strictly preserving the length constraint $|\mathbf{d}| = 1$. Given \mathbf{u}^{n-1} , \mathbf{d}^{n-1} , p^{n-1} , \mathbf{u}^n , \mathbf{d}^n , and p^n , the solution at t^{n+1} is computed through the following steps:

– *Step 1* (Predictor): Find \mathbf{d}_*^{n+1} satisfying

$$\frac{3\mathbf{d}_*^{n+1} - 4\mathbf{d}^n + \mathbf{d}^{n-1}}{2\delta t} = -(\mathbf{u}^n \cdot \nabla)\mathbf{d}_*^{n+1} + \gamma \Delta \mathbf{d}_*^{n+1} + \gamma q^n \mathbf{d}^n. \quad (3.16)$$

– *Step 2* (Corrector): Find $(\mathbf{d}^{n+1}, q^{n+1})$ satisfying

$$\frac{3\mathbf{d}^{n+1} - 3\mathbf{d}_*^{n+1}}{2\delta t} = \gamma q^{n+1} \mathbf{d}^{n+1} - \gamma q^n \mathbf{d}^n, \quad (3.17)$$

$$|\mathbf{d}^{n+1}| = 1. \quad (3.18)$$

– Step 3: Find \mathbf{u}_*^{n+1} satisfying

$$\begin{aligned} \frac{3\mathbf{u}_*^{n+1} - 4\mathbf{u}^n + \mathbf{u}^{n-1}}{2\delta t} + (\mathbf{u}^n \cdot \nabla)\mathbf{u}_*^{n+1} - \nu\Delta\mathbf{u}_*^{n+1} + \nabla p^n \\ + \lambda(\nabla\mathbf{d}^{n+1})^t \Delta\mathbf{d}^{n+1} = 0, \quad \mathbf{u}_*^{n+1}|_{\partial\Omega} = 0. \end{aligned} \tag{3.19}$$

– Step 4: Find $(\mathbf{u}^{n+1}, p^{n+1})$ satisfying

$$\frac{3\mathbf{u}^{n+1} - 3\mathbf{u}_*^{n+1}}{2\delta t} + \nabla(p^{n+1} - p^n + \nu\nabla \cdot \mathbf{u}_*^{n+1}) = 0, \tag{3.20}$$

$$\nabla \cdot \mathbf{u}^{n+1} = 0, \quad \mathbf{u}^{n+1} \cdot \mathbf{n}|_{\partial\Omega} = 0. \tag{3.21}$$

Clearly, \mathbf{d}_*^{n+1} can be directly obtained from Step 1. Next, we demonstrate how to efficiently solve $(\mathbf{d}^{n+1}, q^{n+1})$ in Step 2. Rewriting (3.17) in an equivalent form gives

$$(3 - 2\delta t\gamma q^{n+1})\mathbf{d}^{n+1} = 3\mathbf{d}_*^{n+1} - 2\delta t\gamma q^n \mathbf{d}^n. \tag{3.22}$$

By multiplying both sides of (3.22) by themselves and using (3.18), we obtain

$$(3 - 2\delta t\gamma q^{n+1})^2 = |3\mathbf{d}_*^{n+1} - 2\delta t\gamma q^n \mathbf{d}^n|^2.$$

Following the proof of Theorem 3.1, we can derive a similar result.

Theorem 3.2. *The scheme (3.17) and (3.18) exhibits two distinct sets of solutions. The set of solution consistent with (2.6) and (2.9) is given by*

$$q^{n+1} = \frac{3 - |3\mathbf{d}_*^{n+1} - 2\delta t\gamma q^n \mathbf{d}^n|}{2\gamma\delta t}, \tag{3.23}$$

and

$$\mathbf{d}^{n+1} = \frac{3\mathbf{d}_*^{n+1} - 2\delta t\gamma q^n \mathbf{d}^n}{|3\mathbf{d}_*^{n+1} - 2\delta t\gamma q^n \mathbf{d}^n|}. \tag{3.24}$$

Obviously, the solution of scheme (3.37) and (3.38) is given by

$$q^{n+1} = \frac{3 - |3\mathbf{d}_*^{n+1} - 2\delta t\gamma q^n \mathbf{d}^n|}{2\delta t}, \quad \mathbf{d}^{n+1} = \frac{3\mathbf{d}_*^{n+1} - 2\delta t\gamma q^n \mathbf{d}^n}{|3\mathbf{d}_*^{n+1} - 2\delta t\gamma q^n \mathbf{d}^n|}.$$

Remark 3.2. Considering (3.20) and (3.21), we decouple \mathbf{u}^{n+1} and p^{n+1} by the following steps: Taking divergence on both sides of the equation (3.20) at the same time:

$$\Delta(p^{n+1} - p^n) = \frac{3}{2\delta t} \nabla \cdot \mathbf{u}_*^{n+1} - \nabla \cdot \nabla(\nu\nabla \cdot \mathbf{u}_*^{n+1}). \tag{3.25}$$

In the end, \mathbf{u}^{n+1} is updated by

$$\mathbf{u}^{n+1} = \mathbf{u}_*^{n+1} - \frac{2}{3}\delta t\nabla(p^{n+1} - p^n) - \frac{2\delta t}{3}\nabla(\nu\nabla \cdot \mathbf{u}_*^{n+1}). \tag{3.26}$$

3.1.3. LM-I Crank-Nicolson scheme (LM-I-CN)

Alternative length preserving methods can be developed using other second-order time discretization schemes. For example, the Crank-Nicolson (CN) scheme provides an efficient and accurate approach for achieving second-order temporal accuracy. Similar to the LM-I-BDF2 scheme, the CN scheme can be incorporated within the same predictor-corrector framework. In the following, we present the length preserving scheme based on CN for solving the system (2.6)–(2.9). Given \mathbf{u}^n , \mathbf{d}^n and p^n , the solution at t^{n+1} is computed through the following steps:

- Step 1 (Predictor): Find \mathbf{d}_*^{n+1} satisfying

$$\frac{\mathbf{d}_*^{n+1} - \mathbf{d}^n}{\delta t} = -(\mathbf{u}^n \cdot \nabla) \frac{\mathbf{d}_*^{n+1} + \mathbf{d}^n}{2} + \gamma \Delta \frac{\mathbf{d}_*^{n+1} + \mathbf{d}^n}{2} + \gamma q^n \mathbf{d}^n. \tag{3.27}$$

- Step 2 (Corrector): Find $(\mathbf{d}^{n+1}, q^{n+1})$

$$\frac{\mathbf{d}^{n+1} - \mathbf{d}_*^{n+1}}{\delta t} = \gamma \frac{q^{n+1} \mathbf{d}^{n+1} - q^n \mathbf{d}^n}{2}, \tag{3.28}$$

$$|\mathbf{d}^{n+1}| = 1. \tag{3.29}$$

- Step 3: Find \mathbf{u}_*^{n+1} satisfying

$$\begin{aligned} \frac{\mathbf{u}_*^{n+1} - \mathbf{u}^n}{\delta t} + (\mathbf{u}^n \cdot \nabla) \frac{\mathbf{u}_*^{n+1} + \mathbf{u}^n}{2} - \nu \Delta \left(\frac{\mathbf{u}_*^{n+1} + \mathbf{u}^n}{2} \right) + \nabla p^n \\ + \lambda (\nabla \mathbf{d}^{n+1})^t \Delta \mathbf{d}^{n+1}, \quad \mathbf{u}_*^{n+1}|_{\partial\Omega} = 0. \end{aligned} \tag{3.30}$$

- Step 4: Find $(\mathbf{u}^{n+1}, p^{n+1})$ satisfying

$$\frac{\mathbf{u}^{n+1} - \mathbf{u}_*^{n+1}}{\delta t} + \frac{1}{2} \nabla (p^{n+1} - p^n) = 0, \tag{3.31}$$

$$\nabla \cdot \mathbf{u}^{n+1} = 0, \quad \mathbf{u}^{n+1} \cdot \mathbf{n}|_{\partial\Omega} = 0. \tag{3.32}$$

Obviously, (3.28) and (3.29) can be solved similarly to (3.17) and (3.18), the solution is given by

$$q^{n+1} = \frac{2 - |2\mathbf{d}_*^{n+1} - \delta t \gamma q^n \mathbf{d}^n|}{2\gamma \delta t}, \quad \mathbf{d}^{n+1} = \frac{2\mathbf{d}_*^{n+1} - \delta t \gamma q^n \mathbf{d}^n}{|2\mathbf{d}_*^{n+1} - \delta t \gamma q^n \mathbf{d}^n|}.$$

3.2. Length preserving schemes *via* Lagrange multiplier II

We further propose a class of fully decoupled and length preserving semi-discrete schemes for the system (2.10)–(2.13), where the Lagrange multiplier $q(\mathbf{x}, t)$ is identically zero at the continuous level and is introduced only at the discrete level to enforce the length constraint. Under the predictor-corrector framework, the resulting scheme is fully decoupled, enabling an efficient and stable numerical implementation.

3.2.1. LM-II first-order scheme (LM-II-1st)

We present a first-order length preserving semi-discrete scheme for the system (2.10)–(2.13). Given \mathbf{u}^n , \mathbf{d}^n , and p^n , the solution at t^{n+1} is computed by the following steps:

- Step 1 (Predictor): Find \mathbf{d}_*^{n+1} satisfying

$$\frac{\mathbf{d}_*^{n+1} - \mathbf{d}^n}{\delta t} = -(\mathbf{u}^n \cdot \nabla) \mathbf{d}^n + \gamma (\Delta \mathbf{d}_*^{n+1} + |\nabla \mathbf{d}^n|^2 \mathbf{d}^n). \tag{3.33}$$

– *Step 2* (Corrector): Find $(\mathbf{d}^{n+1}, q^{n+1})$

$$\frac{\mathbf{d}^{n+1} - \mathbf{d}_*^{n+1}}{\delta t} = q^{n+1} \mathbf{d}^{n+1}, \tag{3.34}$$

$$|\mathbf{d}^{n+1}| = 1. \tag{3.35}$$

– *Step 3*: Find \mathbf{u}_*^{n+1} satisfying equation (3.4).
 – *Step 4*: Find $(\mathbf{u}^{n+1}, p^{n+1})$ satisfying equations (3.5) and (3.6).

Similarly to (3.2) and (3.3), we can show that the above system (3.34) and (3.35) admits two sets of solution and the one which is consistent to (2.10) and (2.13) is given by

$$q^{n+1} = \frac{1 - |\mathbf{d}_*^{n+1}|}{\delta t}, \quad \mathbf{d}^{n+1} = \frac{\mathbf{d}_*^{n+1}}{|\mathbf{d}_*^{n+1}|}.$$

3.2.2. *LM-II second-order backward difference formula scheme (LM-II-BDF2)*

We present a second-order length preserving semi-discrete scheme for the system (2.10)–(2.13), based on the backward difference formula. This scheme inherits the decoupled structure of LM-II-1st while achieving higher temporal accuracy. Given $\mathbf{u}^{n-1}, \mathbf{d}^{n-1}, p^{n-1}, \mathbf{u}^n, \mathbf{d}^n$, and p^n , the solution at t^{n+1} is computed by the following steps:

– *Step 1* (Predictor): Find \mathbf{d}_*^{n+1} satisfying

$$\frac{3\mathbf{d}_*^{n+1} - 4\mathbf{d}^n + \mathbf{d}^{n-1}}{2\delta t} = -(\mathbf{u}^n \cdot \nabla)\mathbf{d}_*^{n+1} + \gamma\Delta\mathbf{d}_*^{n+1} + \gamma|\nabla\mathbf{d}^n|^2\mathbf{d}_*^{n+1} + q^n\mathbf{d}^n. \tag{3.36}$$

– *Step 2* (Corrector): Find $(\mathbf{d}^{n+1}, q^{n+1})$ satisfying

$$\frac{3\mathbf{d}^{n+1} - 3\mathbf{d}_*^{n+1}}{2\delta t} = q^{n+1}\mathbf{d}^{n+1} - q^n\mathbf{d}^n, \tag{3.37}$$

$$|\mathbf{d}^{n+1}| = 1. \tag{3.38}$$

– *Step 3*: Find \mathbf{u}_*^{n+1} satisfying equation (3.19).
 – *Step 4*: Find $(\mathbf{u}^{n+1}, p^{n+1})$ satisfying equations (3.20) and (3.21).

Similarly to the proof of Theorem 3.2, the solution of the above scheme (3.37) and (3.38) is given by

$$q^{n+1} = \frac{3 - |3\mathbf{d}_*^{n+1} - 2\delta tq^n\mathbf{d}^n|}{2\delta t}, \quad \mathbf{d}^{n+1} = \frac{3\mathbf{d}_*^{n+1} - 2\delta tq^n\mathbf{d}^n}{|3\mathbf{d}_*^{n+1} - 2\delta tq^n\mathbf{d}^n|}.$$

3.2.3. *LM-II Crank-Nicolson scheme (LM-II-CN)*

We now present a second-order, length-preserving semi-discrete scheme based on the CN time discretization. Similar to the LM-II-BDF2 scheme, this method features a fully decoupled structure and enforces the length constraint on the director field exactly at the discrete level. Given $\mathbf{u}^n, \mathbf{d}^n$, and p^n , the solution at t^{n+1} is obtained through the following steps:

– *Step 1* (Predictor): Find \mathbf{d}_*^{n+1} satisfying

$$\frac{\mathbf{d}_*^{n+1} - \mathbf{d}^n}{\delta t} = -(\mathbf{u}^n \cdot \nabla)\frac{\mathbf{d}_*^{n+1} + \mathbf{d}^n}{2} + \gamma\Delta\frac{\mathbf{d}_*^{n+1} + \mathbf{d}^n}{2} + \gamma|\nabla\mathbf{d}^n|^2\mathbf{d}^n + q^n\mathbf{d}^n. \tag{3.39}$$

– *Step 2* (Corrector): Find $(\mathbf{d}^{n+1}, q^{n+1})$

$$\frac{\mathbf{d}^{n+1} - \mathbf{d}_*^{n+1}}{\delta t} = \frac{q^{n+1} \mathbf{d}^{n+1} - q^n \mathbf{d}^n}{2}, \tag{3.40}$$

$$|\mathbf{d}^{n+1}| = 1. \tag{3.41}$$

– *Step 3*: Find \mathbf{u}_*^{n+1} satisfying equation (3.30).

– *Step 4*: Find $(\mathbf{u}^{n+1}, p^{n+1})$ satisfying equations (3.31) and (3.32).

Obviously, the solution of the above scheme (3.40) and (3.41) is given by

$$q^{n+1} = \frac{2 - |2\mathbf{d}_*^{n+1} - \delta t \gamma q^n \mathbf{d}^n|}{2\gamma \delta t}, \quad \mathbf{d}^{n+1} = \frac{2\mathbf{d}_*^{n+1} - \delta t \gamma q^n \mathbf{d}^n}{|2\mathbf{d}_*^{n+1} - \delta t \gamma q^n \mathbf{d}^n|}.$$

4. NUMERICAL EXPERIMENTS

In this section, we evaluate the convergence rate, stability, and energy dissipation properties of the proposed LM-I and LM-II semi-discrete schemes through a series of numerical experiments. Additionally, we reproduce the numerical examples from [1] to further validate the accuracy and reliability of the proposed schemes. For the spatial discretisation, we employ the stable Taylor-Hood finite element pair $P^2 - P^1$ to solve the Ericksen–Leslie model (2.1)–(2.4). Specifically, the P^2 finite element space is used for approximating the director field \mathbf{d} and the velocity field \mathbf{u} , while the P^1 space is used for the pressure p . Under this spatial discretisation, the schemes achieve second-order accuracy in space for both \mathbf{d} and \mathbf{u} in H^1 -norm, and for p in L^2 -norm. All simulations were performed on a workstation equipped with a 12th Gen Intel® Core™ i9-12900K CPU and 128 GB RAM, running Ubuntu 22.04.1 LTS. The numerical codes were implemented and executed using FreeFem++ 4.5.

Example 4.1 (Convergence test). We consider the Ericksen–Leslie model (2.1)–(2.4) in the domain $\Omega = [0, 1]^2$, subject to the following initial conditions:

$$\begin{cases} \mathbf{d}_0 = (\sin(a), \cos(a))^t, & a := 2.0\pi(\cos(x) - \sin(y)), \\ \mathbf{u}_0 = (0, 0)^t, \\ p_0 = 0. \end{cases}$$

The physical parameters are set as $\nu = 0.1, \lambda = 1, \gamma = 1$.

For both the LM-I-1st and LM-II-1st schemes, first-order temporal accuracy is expected, *i.e.*, the error behaves as $O(h^2 + \Delta t)$. To investigate the temporal convergence, the spatial mesh is fixed with size $h = 1/30$, while the time step is refined according to $\delta t = \frac{0.001}{2^{l-1}}$, with $l = 1, \dots, 5$. The Cauchy differences are computed at the final time $t^{n+1} = (n + 1)\delta t = 0.1$ for the components $v = d_1, d_2, u_1, u_2, p$, where $\mathbf{d} = (d_1, d_2)^T$ and $\mathbf{u} = (u_1, u_2)^T$. Specifically, we calculate $v_{l+1}^{n+1} - v_l^{n+1}, l = 1, \dots, 4$. The numerical results are reported in Tables 1 and 2, and confirm that both the LM-I-1st and LM-II-1st schemes achieve the expected first-order convergence in time.

For the second-order schemes, the numerical error satisfies the estimate $O(h^2 + \Delta t^2) = O(\Delta t^2)$. To verify the theoretical convergence order, we conduct numerical experiments on five successively refined meshes with size $h = \frac{\sqrt{2}}{5 \times 2^{l-1}}, l = 1, \dots, 5$. The time step is defined as $\delta t = \frac{0.005}{\sqrt{2}} h$, ensuring a consistent relationship between spatial and temporal discretization. The Cauchy differences are computed at the final time $t^{n+1} = 0.1$. As reported in Tables 3 and 4, both the LM-I-BDF2 and LM-I-CN schemes exhibit second-order convergence. Similarly, the result in Tables 5 and 6 confirm the second-order accuracy of the LM-II-BDF2 and LM-II-CN schemes.

Example 4.2. Referring to the numerical experiments on smooth solutions in [1], the Ericksen–Leslie model (2.1)–(2.4) is considered in the domain $\Omega = [-1, 1]^2$. The initial conditions and physical parameters are adopted from Example 4.1. To ensure consistency, the spatial mesh size and time step are fixed as $h = 1/25$ and $\delta t = 2.5 \times 10^{-4}$, respectively.

TABLE 1. Example 4.1, Cauchy convergence test for the LM-I-1st scheme.

l	$\ \nabla \mathbf{d}_{l+1}^{n+1} - \nabla \mathbf{d}_l^{n+1}\ $	Rate	$\ \nabla \mathbf{u}_{l+1}^{n+1} - \nabla \mathbf{u}_l^{n+1}\ $	Rate	$\ p_{l+1}^{n+1} - p_l^{n+1}\ $	Rate
1	0.03527831861	–	0.05196539498	–	0.06916545715	–
2	0.01785030108	0.98	0.0258904586	1.00	0.03453726001	1.00
3	0.008988163726	0.99	0.01291747907	1.00	0.01727144006	1.00
4	0.004517015514	0.99	0.006448850257	1.00	0.008647857238	1.00

TABLE 2. Example 4.1, Cauchy convergence test for the LM-II-1st scheme.

l	$\ \nabla \mathbf{d}_{l+1}^{n+1} - \nabla \mathbf{d}_l^{n+1}\ $	Rate	$\ \nabla \mathbf{u}_{l+1}^{n+1} - \nabla \mathbf{u}_l^{n+1}\ $	Rate	$\ p_{l+1}^{n+1} - p_l^{n+1}\ $	Rate
1	0.01651120543	–	0.02063816617	–	0.03172011263	–
2	0.008313781656	0.99	0.01036340852	0.99	0.01587838663	1.00
3	0.004172851763	0.99	0.005187165697	1.00	0.007945228878	1.00
4	0.002096529558	0.99	0.002589103149	1.01	0.003983174813	1.00

TABLE 3. Example 4.1, Cauchy convergence test for the LM-I-BDF2 scheme.

l	$\ \nabla \mathbf{d}_{l+1}^{n+1} - \nabla \mathbf{d}_l^{n+1}\ $	Rate	$\ \nabla \mathbf{u}_{l+1}^{n+1} - \nabla \mathbf{u}_l^{n+1}\ $	Rate	$\ p_{l+1}^{n+1} - p_l^{n+1}\ $	Rate
1	0.07664840508	–	0.1002339368	–	0.0292118028	–
2	0.01834678732	2.06	0.0276481446	1.86	0.00794947932	1.89
3	0.004610362919	1.99	0.007235607133	1.93	0.002050580738	1.95
4	0.001155446382	2.00	0.001832291291	1.98	0.0005306368593	1.95

TABLE 4. Example 4.1, Cauchy convergence test for the LM-I-CN scheme.

l	$\ \nabla \mathbf{d}_{l+1}^{n+1} - \nabla \mathbf{d}_l^{n+1}\ $	Rate	$\ \nabla \mathbf{u}_{l+1}^{n+1} - \nabla \mathbf{u}_l^{n+1}\ $	Rate	$\ p_{l+1}^{n+1} - p_l^{n+1}\ $	Rate
1	0.07853985108	–	0.09378690467	–	0.02672629102	–
2	0.01839233768	2.09	0.02736425643	1.78	0.006748642847	1.99
3	0.004611446787	2.00	0.007061102603	1.95	0.001806142945	1.90
4	0.001155544998	2.00	0.001776015526	1.99	0.0005130106436	1.82

TABLE 5. Example 4.1, Cauchy convergence test for the LM-II-BDF2 scheme.

l	$\ \nabla \mathbf{d}_{l+1}^{n+1} - \nabla \mathbf{d}_l^{n+1}\ $	Rate	$\ \nabla \mathbf{u}_{l+1}^{n+1} - \nabla \mathbf{u}_l^{n+1}\ $	Rate	$\ p_{l+1}^{n+1} - p_l^{n+1}\ $	Rate
1	0.07749897082	–	0.09983993251	–	0.02953744349	–
2	0.0183405143	2.08	0.02768927216	1.85	0.007941286413	1.90
3	0.004611096788	1.99	0.007239674694	1.94	0.002043414144	1.96
4	0.001155719875	2.00	0.001831906674	1.98	0.0005288949313	1.95

TABLE 6. Example 4.1, Cauchy convergence test for the LM-II-CN scheme.

l	$\ \nabla \mathbf{d}_{l+1}^{n+1} - \nabla \mathbf{d}_l^{n+1}\ $	Rate	$\ \nabla \mathbf{u}_{l+1}^{n+1} - \nabla \mathbf{u}_l^{n+1}\ $	Rate	$\ p_{l+1}^{n+1} - p_l^{n+1}\ $	Rate
1	0.07880540491	–	0.09343616445	–	0.02693728222	–
2	0.01835816884	2.10	0.02712035973	1.78	0.006417409357	2.07
3	0.004804742477	1.93	0.0068224642	1.99	0.00159266084	2.01
4	0.001348631051	1.83	0.001638290334	2.06	0.0004003749312	1.99

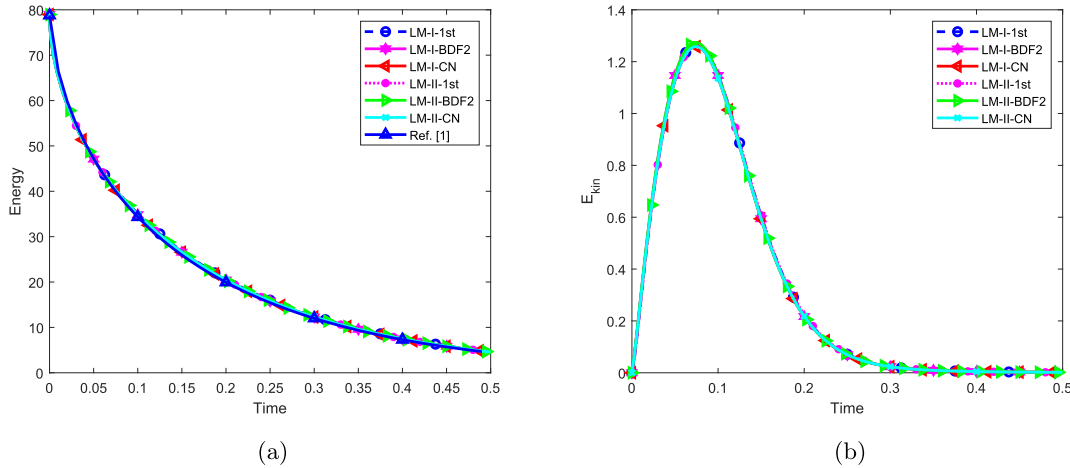


FIGURE 1. Example 4.2, total and kinetic energy curves computed by LM-I and LM-II schemes. (a) Total energy. (b) Kinetic energy.

Simulations are performed using both the first-order and second-order schemes introduced previously, including the LM-I-1st, LM-II-1st, LM-I-BDF2, LM-II-BDF2, LM-I-CN, and LM-II-CN. The total energy E evolution curves, presented in Figure 1a, exhibit consistent energy dissipation across all cases, in good agreement with the findings reported in [1]. This observation confirms the stability and accuracy of the proposed schemes in preserving the physical structure of the model. Furthermore, the kinetic energy, defined as $E_{kin} = \frac{1}{2}\|u\|^2$, is examined in Figure 1b to provide a more detailed understanding of the system dynamics. These results demonstrate that the proposed schemes accurately capture the energy dissipation behavior while maintaining the essential physical properties of the model.

We further compare the CPU times of the LM-I-BDF2 and LM-II-BDF2 schemes under the same computational settings as those in [1], with time step $\delta t = 0.01$ and mesh size $h = 1/32$. All linear systems are solved using the UMFPAK solver in FreeFem++. For the implicit scheme reported in [1], Newton’s method is employed with a tolerance of 10^{-6} . As summarized in Table 7, the proposed schemes significantly reduce computational cost, requiring only 0.6% of the original runtime and thereby demonstrating superior efficiency.

Example 4.3. Following the numerical experiments in [14], we consider the Ericksen–Leslie model (2.1)–(2.4) in the domain $\Omega = \{x^2 + y^2 < 1\}$. The initial data are prescribed as follows:

$$\begin{cases} \mathbf{d}_0 = (\sin(a), \cos(a))^t, & a := 4\pi(x^4 - y^4)^2, \\ \mathbf{u}_0 = (0, 0)^t, \\ p_0 = 0. \end{cases}$$

TABLE 7. Example 4.2, the CPU time is also quantified as a percentage (PCT) relative to the implicit method in [1].

Scheme	CPU times for Example 4.2	PCT
Ref. [1]	10 163.9 s	100.0%
LM-I-BDF2	56.3337 s	0.6%
LM-II-BDF2	57.9093 s	0.6%

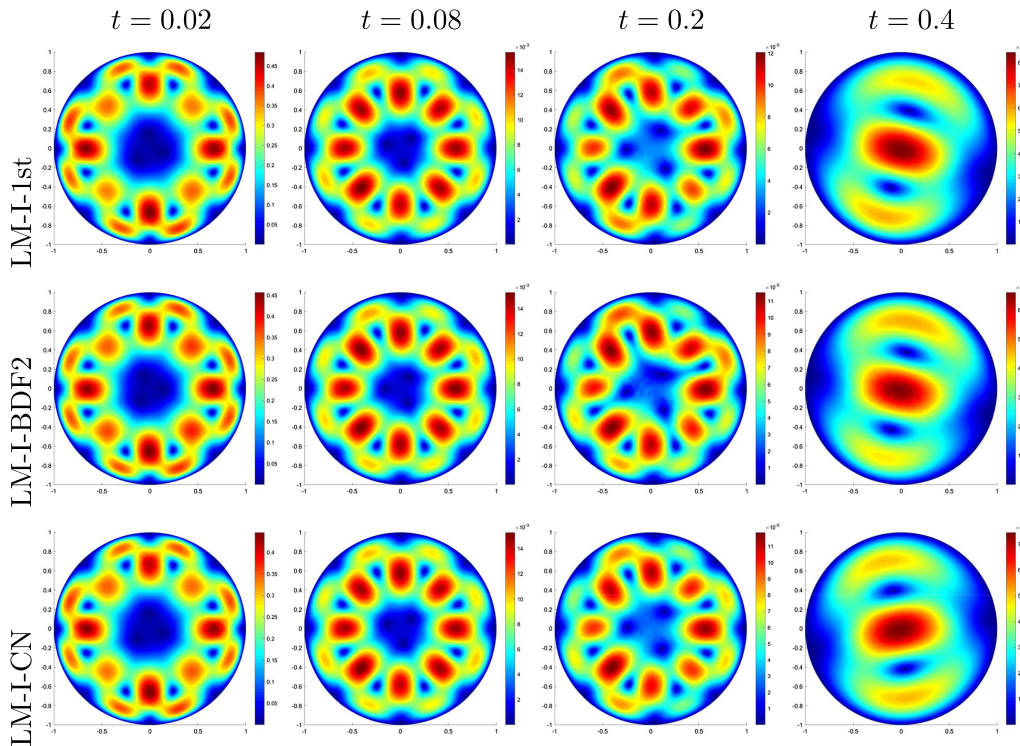


FIGURE 2. Example 4.3, snapshots of the vector magnitude $|\mathbf{u}|$ obtained using the LM-I schemes at $t = 0.02, 0.08, 0.2, 0.4$.

The physical parameters are set as $\lambda = 1, \gamma = 1$ and $\nu = 2$. All simulations are performed using the proposed schemes with a uniform time step $\delta t = 10^{-4}$.

We now present the numerical results obtained using the LM-I and LM-II schemes. Figures 2 and 3 display the time evolution of the velocity magnitude $|\mathbf{u}|$ computed by each scheme, while Figures 4 and 5 show the corresponding dynamics of the director field. The results clearly capture the smooth evolution of both the velocity and director fields. The close agreement between the two schemes further confirms their accuracy and robustness.

The total energy E evolution computed by all six schemes is shown in Figure 6a, indicating that each scheme preserves the intrinsic energy dissipation property of the Ericksen–Leslie model. In addition, the kinetic energy evolution (see Fig. 6b) initially increases and then gradually decays, reflecting the characteristic transfer and dissipation of energy within the system. This behavior further supports the reliability and stability of the

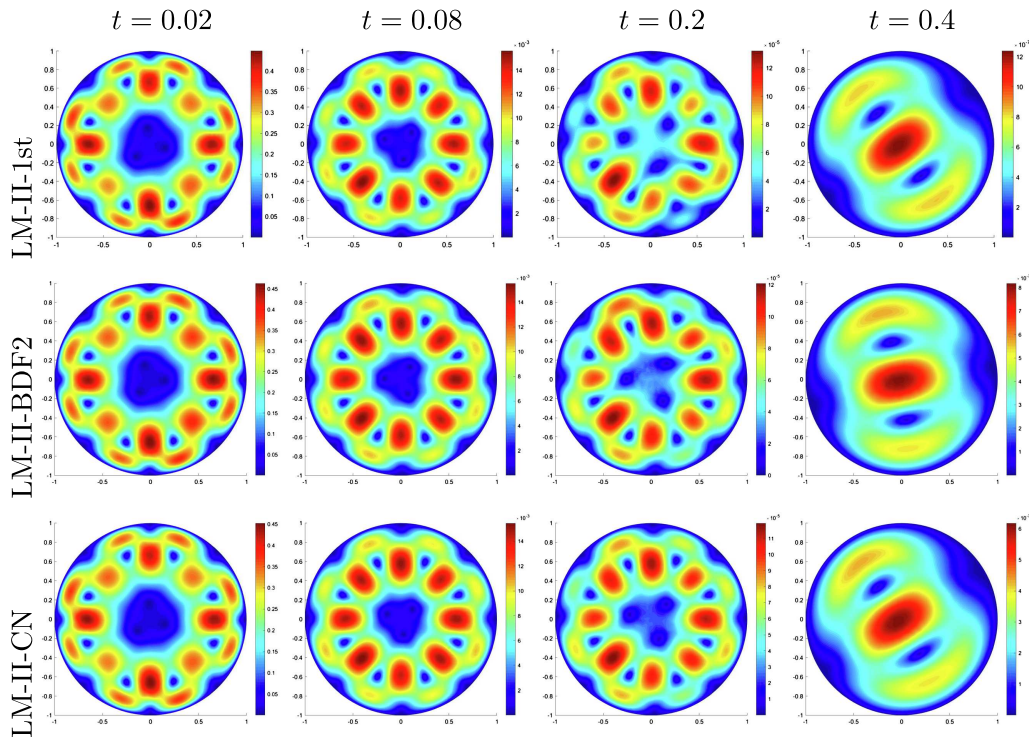


FIGURE 3. Example 4.3, snapshots of the vector magnitude $|\mathbf{u}|$ obtained using the LM-II schemes at $t = 0.02, 0.08, 0.2, 0.4$.

proposed schemes. In summary, these results demonstrate that both the LM-I and LM-II schemes yield stable and accurate solutions while preserving the essential physical properties of the model.

Example 4.4 (Annihilation of the singularities). In this example, we consider the Ericksen–Leslie model (2.1)–(2.4) in a two-dimensional square domain $\Omega = (-1, 1) \times (-1, 1)$, with physical parameters set to $\lambda = 0.01$ and $\nu = \gamma = 1$. The initial conditions are prescribed as follows

$$\begin{cases} \mathbf{d}_0 = \tilde{\mathbf{d}} / \sqrt{|\tilde{\mathbf{d}}|^2 + 0.05^2}, & \text{where } \tilde{\mathbf{d}} = (x^2/0.5^2 + y^2/0.25^2 - 1, -xy), \\ \mathbf{u}_0 = 20(-y, x), \\ p_0 = 0. \end{cases}$$

This numerical example investigates the dynamics of singularities (defects) in liquid crystal flows using the proposed numerical schemes. The simulation focuses on the annihilation process of four initially present topological defects, and captures the intricate interactions among the director field \mathbf{d} , the velocity field \mathbf{u} , and the system’s energy dissipation. The initial director field \mathbf{d}_0 introduces four singularities in the domain, while the initial velocity field \mathbf{u}_0 represents a rotational flow. This setup generates a highly dynamic environment for observing defect interaction and evolution under hydrodynamic coupling. Figure 7 shows the time evolution of the director field \mathbf{d} at $t = 0, 0.02, 0.06, 0.08$, and 0.25 , while Figure 8 displays corresponding velocity fields at $t = 0.02, 0.06, 0.08, 0.25$, and 0.8 , computed by the LM-I-CN scheme. At the initial time $t = 0$, the director field exhibits four singularities located at $(\pm\frac{1}{2}, 0)$ and $(0, \pm\frac{1}{4})$, as shown in Figure 7a. These defects originate from the initial configuration of \mathbf{d} , which disrupts the uniform alignment of the liquid crystal. At $t = 0.02$, the velocity field induces a rotational flow (see Fig. 8a) that drives the motion of these singularities. This rotational

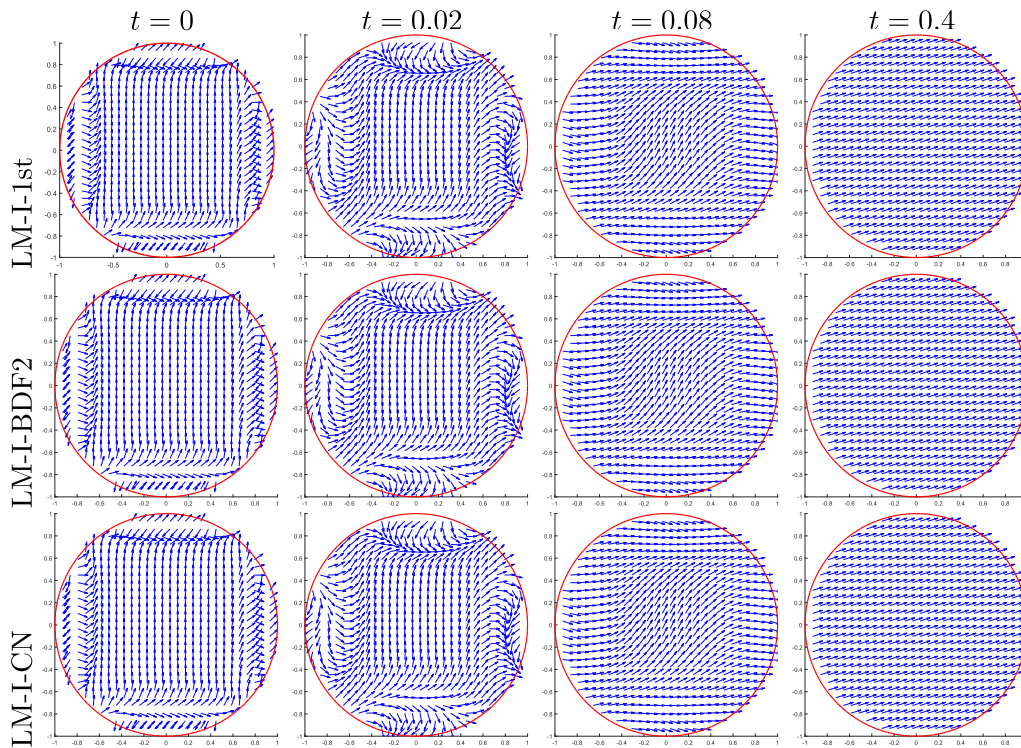


FIGURE 4. Example 4.3, snapshots of the director field \mathbf{d} obtained using the LM-I schemes at $t = 0, 0.02, 0.08, 0.4$.

flow drives the defects around the origin (see Fig. 7b), leading to dynamic interactions among them. Over time, the dissipative nature of the system causes these defects gradually merge and eventually annihilate, resulting in a nearly uniform director field at $t = 0.25$ (see Fig. 7e). The corresponding evolution of the total energy E is shown in Figure 9, which reveals a rapid decrease in energy and confirms that the proposed scheme respects the intrinsic energy dissipation law of the Ericksen–Leslie model. These results highlight the capability of the proposed schemes to robustly capture the complex defect dynamics while accurately preserving the physical structure of the model, particularly the energy dissipation property.

Example 4.5. In this example, we compare the LM-I and LM-II schemes for the Ericksen–Leslie model (2.1)–(2.4) in terms of stability and accuracy under the initial condition (4.1).

As shown in Figure 10, we depict the energy evolution computed by all schemes with different time steps. In Figures 10a and 10b, we observe that both LM-I and LM-II schemes are stable and accurately capture the dynamics of the Ericksen–Leslie model with time steps $\delta t = 5.0 \times 10^{-4}, 10^{-3}$. However, Figure 10c indicates that the LM-II schemes can produce more accurate energy curves than the LM-I schemes at the larger time step $\delta t = 5.0 \times 10^{-3}$. Figure 11 shows the numerical solutions \mathbf{d} at $t = 0, 0.01, 0.1, 0.2, 0.4$ computed by the LM-II-BDF2 scheme.

5. CONCLUSION

In this paper, we proposed two types of linear and fully decoupled numerical schemes for the Ericksen–Leslie model, based on the Lagrange multiplier approach. These schemes enforce the length constraint on the director

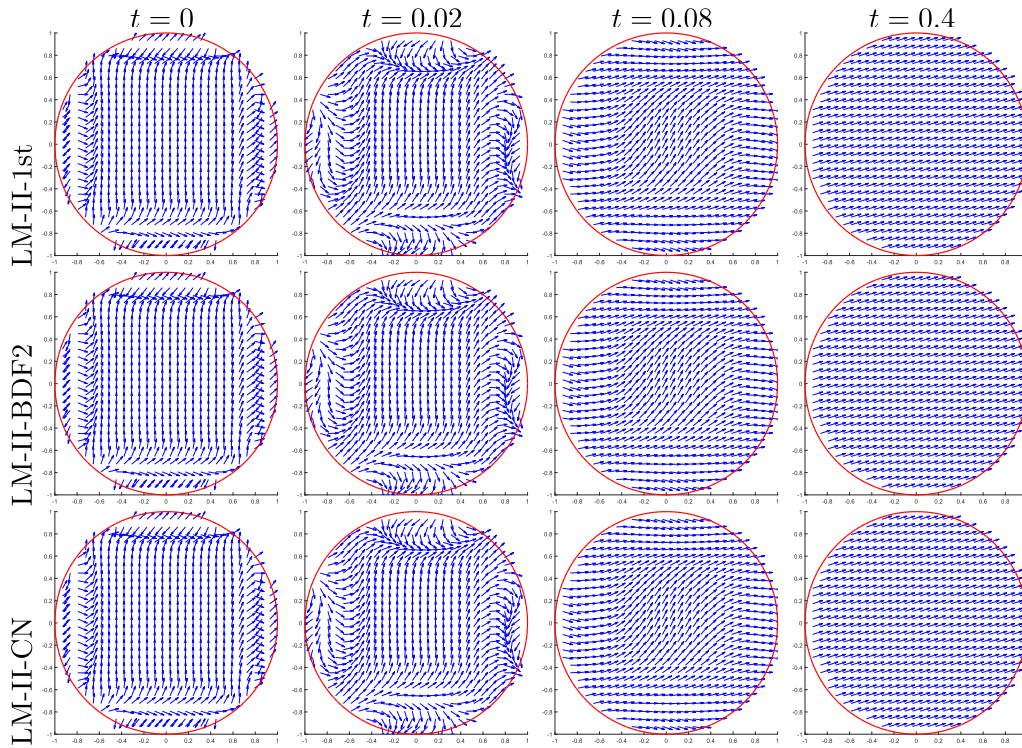


FIGURE 5. Example 4.3, snapshots of the director field \mathbf{d} obtained using the LM-II schemes at $t = 0, 0.02, 0.08, 0.4$.

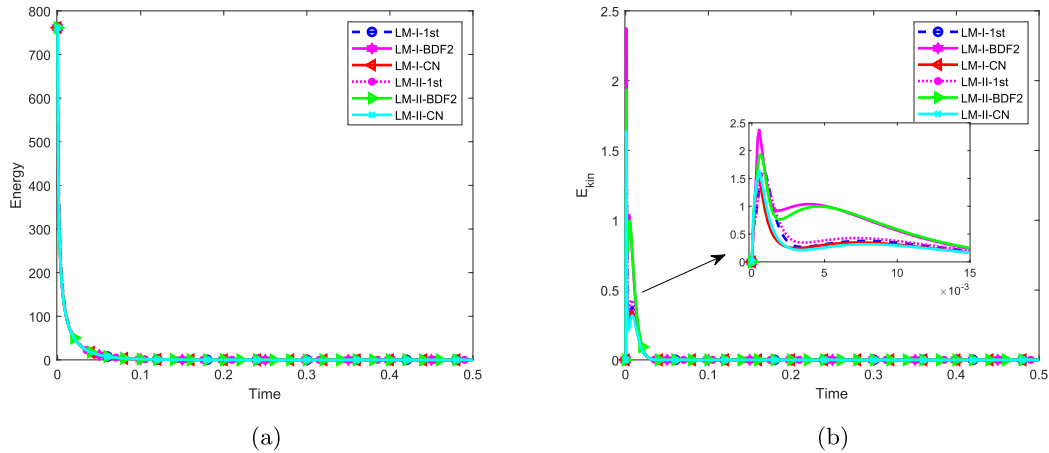


FIGURE 6. Example 4.3, total and kinetic energy curves computed by the LM-I and LM-II schemes. (a) Total energy. (b) Kinetic energy.

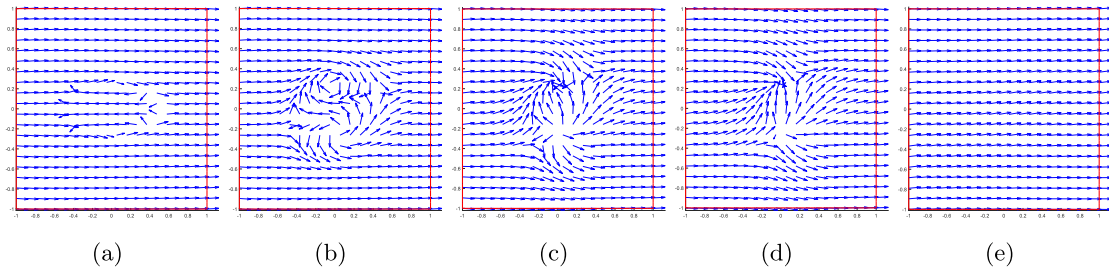


FIGURE 7. Example 4.4, images of the director field \mathbf{d} at $t = 0, 0.02, 0.06, 0.08, 0.25$ computed by the LM-I-CN scheme.

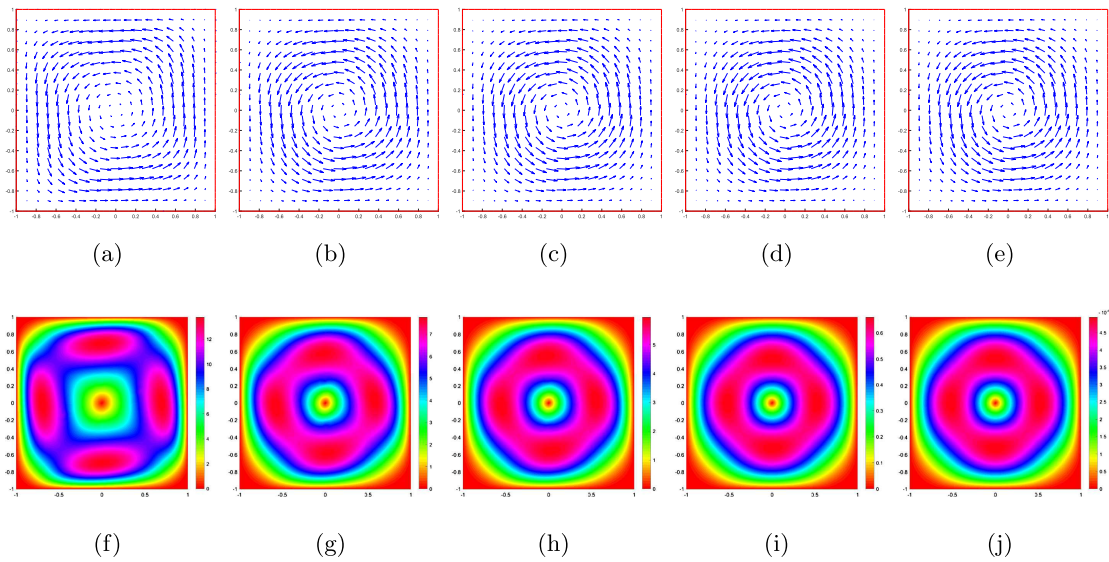


FIGURE 8. Example 4.4, images of the velocity \mathbf{u} (first row) and $|\mathbf{u}|$ (second row) at $t = 0.02, 0.06, 0.08, 0.25, 0.8$ computed by the LM-I-CN scheme.

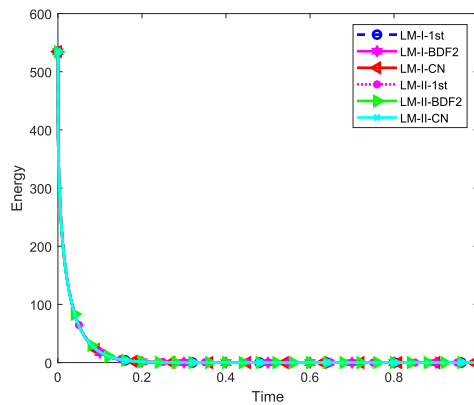


FIGURE 9. Example 4.4, total energy of singularities annihilation by the LM-I-CN scheme.

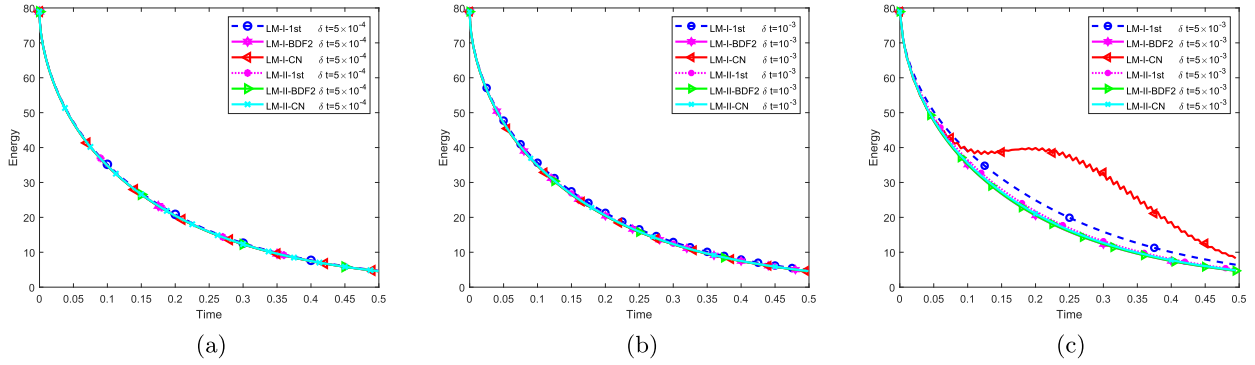


FIGURE 10. Example 4.5, energy comparison for LM-I and LM-II schemes using various time steps. (a) LM-I and LM-II schemes with $\delta t = 5.0 \times 10^{-4}$. (b) LM-I and LM-II schemes with $\delta t = 10^{-3}$. (c) LM-I and LM-II schemes with $\delta t = 5.0 \times 10^{-3}$.

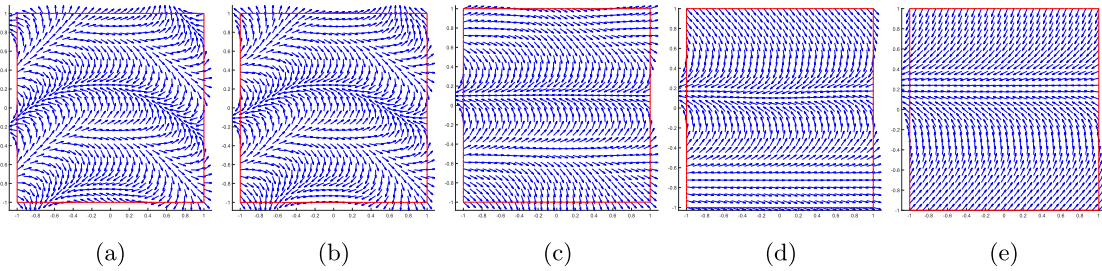


FIGURE 11. Example 4.5, images of the director field \mathbf{d} at $t = 0, 0.01, 0.1, 0.2, 0.4$ computed by the LM-II-BDF2 scheme with $\delta t = 5.0 \times 10^{-3}$.

field and maintain computational efficiency through a linear predictor-corrector framework. We conducted some numerical experiments to assess the stability and accuracy of the proposed schemes, and to compare their performance with the existing method. It is observed that our LM-I and LM-II schemes can perform numerical simulations accurately and efficiently. We also observe that the LM-II schemes, based on a Lagrange multiplier $q(\mathbf{x}, t) = 0$ at the continuous level, generally produce more accurate dynamical approximation than the LM-I schemes, which are based on the Lagrange multiplier $q(\mathbf{x}, t) = |\nabla \mathbf{d}|^2$.

The unconditional stability analysis of the proposed semi-discrete schemes remains a challenging problem. In our future research, we plan to investigate the fully discrete version of the proposed schemes, and perform a detailed stability analysis and error estimates.

FUNDING

Yi’s research was partially supported by NSFC Project (12431014), Project of Scientific Research Fund of the Hunan Provincial Science and Technology Department (2024ZL5017), Postgraduate Scientific Research Innovation Project of Hunan Province (CX20240056), and Program for Science and Technology Innovative Research Team in Higher Educational Institutions of Hunan Province of China.

DATA AVAILABILITY STATEMENT

The research data associated with this article are included in the article.

REFERENCES

- [1] S. Badia, F. Guillén-González and J.V. Gutiérrez-Santacreu, Finite element approximation of nematic liquid crystal flows using a saddle-point structure. *J. Comput. Phys.* **230** (2011) 1686–1706.
- [2] R. Becker, X. Feng and A. Prohl, Finite element approximations of the Ericksen–Leslie model for nematic liquid crystal flow. *SIAM J. Numer. Anal.* **46** (2008) 1704–1731.
- [3] Q. Cheng and J. Shen, Length preserving numerical schemes for Landau–Lifshitz equation based on Lagrange multiplier approaches. *SIAM J. Sci. Comput.* **45** (2023) A530–A553.
- [4] Q. Du, B. Guo and J. Shen, Fourier spectral approximation to a dissipative system modeling the flow of liquid crystals. *SIAM J. Numer. Anal.* **39** (2001) 735–762.
- [5] J.L. Ericksen, Conservation laws for liquid crystals. *Trans. Soc. Rheol.* **5** (1961) 23–34.
- [6] J.L. Ericksen, Hydrostatic theory of liquid crystals. *Arch. Ration. Mech. Anal.* **9** (1962) 371–378.
- [7] V. Girault and F. Guillén-González, Mixed formulation, approximation and decoupling algorithm for a penalized nematic liquid crystals model. *Math. Comput.* **80** (2011) 781–819.
- [8] R. Glowinski, P. Lin and X.B. Pan, An operator-splitting method for a liquid crystal model. *Comput. Phys. Commun.* **152** (2003) 242–252.
- [9] J.L. Guermond and J. Shen, On the error estimates for the rotational pressure correction projection methods. *Math. Comput.* **73** (2004) 1719–1737.
- [10] F. Guillén-González and J.V. Gutiérrez-Santacreu, A linear mixed finite element scheme for a nematic Ericksen–Leslie liquid crystal model. *ESIAM Math. Model. Numer. Anal.* **47** (2013) 1433–1464.
- [11] F.M. Leslie, Some constitutive equations for anisotropic fluids. *Q. J. Mech. Appl. Math.* **19** (1966) 357–370.
- [12] F.M. Leslie, Some constitutive equations for liquid crystals. *Arch. Ration. Mech. Anal.* **28** (1968) 265–283.
- [13] F.M. Leslie, Theory of flow phenomena in liquid crystals. *Adv. Liq. Cryst.* **4** (1979) 1–81.
- [14] T. Li, P.Z. Huang and Y.N. He, A fully discrete, decoupled scheme with different time steps for approximating nematic liquid crystal flow. *Int. J. Numer. Anal. Mod.* **18** (2021) 811–833.
- [15] F. Lin, Nonlinear theory of defects in nematic liquid crystals phase transition and flow phenomena. *Commun. Pure Appl. Math.* **42** (1989) 789–814.
- [16] F. Lin and C. Liu, Nonparabolic dissipative systems modeling the flow of liquid crystals. *Commun. Pure Appl. Math.* **48** (1995) 501–537.
- [17] P. Lin and C. Liu, Simulations of singularity dynamics in liquid crystal flows: a C^0 finite element approach. *J. Comput. Phys.* **215** (2006) 348–362.
- [18] C. Liu and N.J. Walkington, Approximation of liquid crystal flows. *SIAM J. Numer. Anal.* **37** (2000) 725–741.
- [19] A.D. Rey and M.M. Denn, Dynamical phenomena in liquid-crystalline materials. *Ann. Rev. Fluid Mech.* **34** (2003) 233–266.



Please help to maintain this journal in open access!

This journal is currently published in open access under the Subscribe to Open model (S2O). We are thankful to our subscribers and supporters for making it possible to publish this journal in open access in the current year, free of charge for authors and readers.

Check with your library that it subscribes to the journal, or consider making a personal donation to the S2O programme by contacting subscribers@edpsciences.org.

More information, including a list of supporters and financial transparency reports, is available at <https://edpsciences.org/en/subscribe-to-open-s2o>.